Mask blank defect printability comparison using optical and SEM mask and wafer inspection and bright field actinic mask imaging

Pawitter Mangat[1], Erik Verduijn[1], Obert R. Wood II[1] , Markus P. Benk[2], Antoine Wojdyla[2], and Kenneth A. Goldberg[2]

[1]GLOBALFOUNDRIES, 400 Stonebreak Road, Malta, NY 12020, U.S.A.
[2]Center for X-ray Optics, Lawrence Berkeley National Laboratory, Berkeley, CA 94720 U.S.A.

ABSTRACT

Despite significant enhancements in defect detection using optical and e-beam methodology, the smaller length scales and increasing challenges of future technology nodes motivate ongoing research into the need and associated cost of actinic inspection for EUV masks. This paper reports an extensive study of two EUV patterned masks, wherein the mask blank defectivity was characterized using optical (mask and wafer) methods and bright-field mask imaging (using the SHARP actinic microscope) of previously identified blank defects. We find that the bright field actinic imaging tool microscope captures and images many defects that are not seen by the automated optical inspection of patterned masks and printed wafers. In addition, actinic review reveals the impact of multilayer damage and depicts the printability profile which can be used as an added metric to define the patterned mask repair and defect compensation strategies.

KEYWORDS: EUV Mask, EUV Defect Printability, Actinic Mask imaging

1. INTRODUCTION

As extreme ultraviolet (EUV) lithography continues to be a potential option for future patterning nodes, the EUV mask infrastructure, and defect printability in particular, needs to be better understood [1,2]. This is critical for the integration of EUV into HVM for sub-10 nm node lithography [3]. Due to the lack of patterned mask actinic inspection tools and infrastructure, optical inspection tools are being used to optimize the EUV mask defect inspection[4]. Since the EUV masks are tuned for maximizing reflectivity at 13.5 nm, inspecting at optical wavelengths (193+ nm) does not provide the needed details for all defects that might be printing and eventually missed in the optical inspection. Thus, the key challenges are to detect and image real defects on EUV masks with high enough sensitivity at the actinic wavelength and optimal illumination conditions matching the scanner (0.33 NA) for features that are essential for the 7 nm and smaller node requirements.

Recent development on the EUV actinic blank inspection tool have made significant progress and have been published [5]. Hence, it is critical that the result of actinic blank inspection be validated using EUV-wavelength patterned mask imaging. EUV Aerial Imaging Measurement

System (EUV AIMS) has also been recently demonstrated for the measurement of pattern defects but still does not suffice the need for a full patterned mask inspection [6].

This study was initiated to validate the need for actinic patterned mask inspection and to identify shortcomings of the optical mask inspection of the mask. We have compared measurements of found defects on wafer prints, mask optical inspection, and actinic imaging. Furthermore, it is essential to have updated guidelines for the EUV mask repair of patterned mask defects based on actinic inspection and printability assessment. This will enable higher yielding wafer prints, thus improving the cycle time both for device integration and mask making. Furthermore, the key benefit of the actinic imaging is that it encompasses all types of defects: phase and amplitude, absorber and process adders. But the biggest value comes from identifying the phase defects that are not possible to detect using optical and electron-beam inspection tools. The penetration depth of various inspection strategies have been previously published [7] justifying the need for actinic inspection. Optical inspection tools with DUV illumination wavelength, such as 193 nm, can only penetrate the top three bilayers of the multilayer coating due to strong absorption. This makes them largely blind to hidden defects embedded within the sub-layers of the mask and on the substrate: the so-called *phase defects*.

The motivation for this study is to assess the impact of native blank defect printability using the Mask/Wafer Optical Inspection tools and an Actinic mask Bright-field Imaging tool (SHARP) at Lawrence Berkeley National Laboratory [8]. In addition, we seek to understand the characteristics of the defects that did or did not print, while validating guidelines for defect mitigation for mask making and defect-free printability.

2. EXPERIMENTAL DETAILS

Two EUV patterned masks were used in this study and details of the mask have been previously published [9]. The mask comprises a 10×13 array of lines and spaces (horizontal and vertical) arranged in a checkerboard fashion to maximize the patterned area (100×130 mm) such that majority of defects in the critical areas are captured. The first mask (GREMLIN3-PR) has dense lines pitches of 56, 80 and 104 nm (wafer scale); the second mask (GREMLIN4-LT) has uniform, dense lines with 64-nm pitch (wafer scale). Defect maps from the blank supplier, following Ru deposition and generated by a Lasertec M1350 scattering tool, were used as a reference. No defect mitigation methodologies were implemented during mask making since our goal was to characterize and understand as many defects as possible.

The correlation study between the patterned mask inspection details using KLA 61x and respective wafer printability in an automated mode of operation have been previously published for GREMLIN3-PR [9] and for GREMLIN4-LT [10]. Masks were recently exposed using IMEC's NXE3100, and all measurements were done at the best focus and dose conditions. The printed wafers were inspected with KLA2835 tool and the SEM review of the printed wafer was done on mask repeater defects with KLA eDR7000 tool, primarily at the locations mapped to the

blank defects after aligning the blank and patterned mask with reference co-coordinates, using large blank defects.

The masks were then imaged on the SHARP tool. Alignment methods similar to optical SEM inspection were used for coordinate mapping. SHARP has a customizable Fourier-synthesis illuminator that controls the angular profile of the illumination in a lossless manner. For optimal comparison with wafer printing, SHARP's illuminator is programmed to replicate the imaging conditions used in the scanner, whether monopole, annular, dipole, Quasar, or other specialized pupil fills. For the data collected here, SHARP emulated the *disk fill* illumination conditions used in the NXE3100, with partial coherence $\sigma = 0.81$ at 0.33 4×NA. Bright-field images of the illuminated mask are projected onto an EUV CCD camera with 900× magnification using an off-axis Fresnel zone plate lens that mimics the mask-side solid angle and resolution of the NXE3100.

For each measurement, SHARP collects series of images through focus, typically with 400-nm steps (mask scale). This allows the best-focus image to be selected for comparison, and also reveals the amplitude or phase properties of the defects [11]. The data included here shows that brightfield, actinic imaging of patterned masks is sensitive to all defect types; it emulates printing conditions with proper mask illumination and is highly predictive of the detailed features of the printed defects. Actinic imaging facilitates defect characterization on blanks and on pattered masks, and even in absorber areas. It can be used to measure line properties, such as critical dimension (CD), contrast, image log-slope (ILS), illumination dependence, and changes in the process window for defect sites. These properties make it suitable for repair strategy development [12].

3. RESULTS & DISCUSSION

The Gremlin3-PR mask blank had a total of 35 defects identified using the post-Ru deposition inspection and mapped on the SHARP tool. Based on the defect correlation, 13 defects were outside the patterned mask area but were successfully imaged by SHARP. This indicates that SHARP can be used for imaging defects in un-patterned blank areas in either the reflective or the absorber regions. Figure 1 shows actinic images of defects in absorber regions, identified in blank inspection and then imaged with SHARP. It is evident that the size correlation output from the blank scattering tools (i.e. the pixel value) is not well correlated with the apparent size in the actinic images, in all cases. We believe this type of feedback could be used to improve the level of agreement.
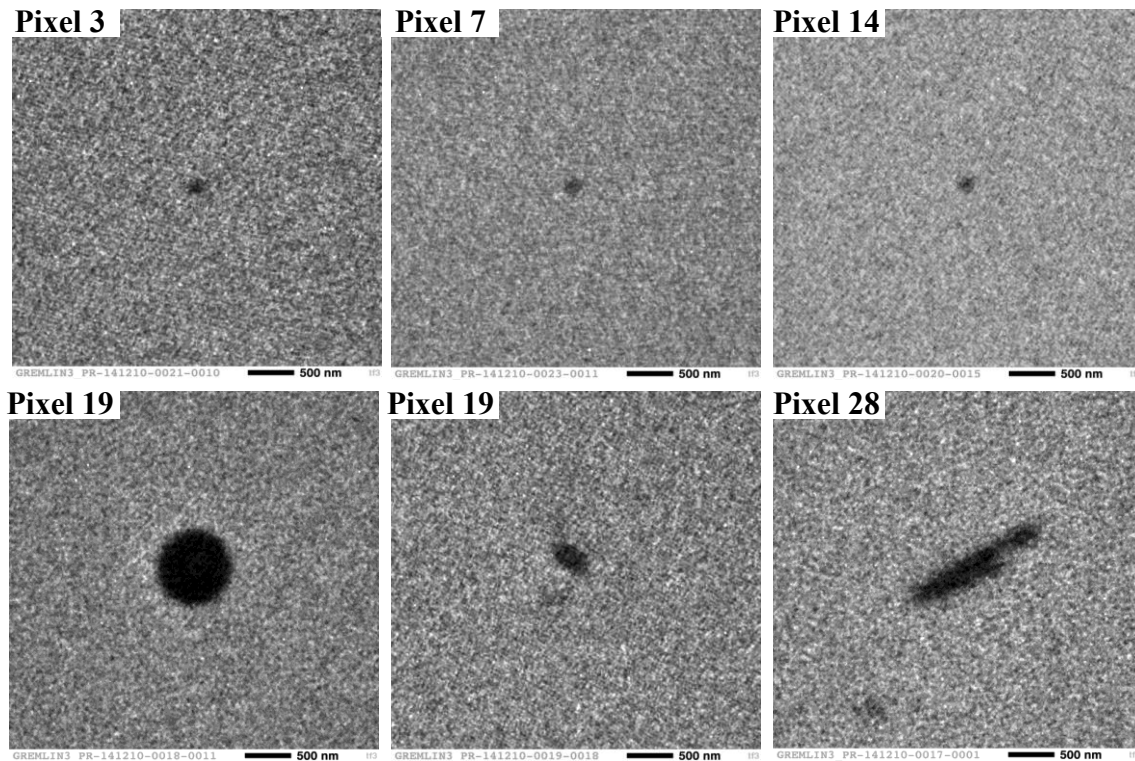
Figure 1. Actinic images of defects in the dark, absorber region of GREMLIN3-PR. The "pixel" values indicate the size assigned by M1350 inspection. Scale bars are all 500 nm.

Within the patterned area, 14 defects were identified and imaged. The majority of these defects were classified as belonging to the smallest pixel bins (i.e. 1 to 4), corresponding to defects below 60 nm. Many of these defects were missed in the previously reported work that was based on just the optical mask and wafer inspection [9]. With the clear appearance of these defects at-wavelength, the actinic imaging shows that pixel 1–4 defects cannot be excluded from the defect mitigation strategies.

There were 4 mask-blank defects that were neither identifiable using the actinic imaging tool nor were they printed on the wafer, indicating that these might be false defects from the blank inspection. There were 4 other defects that were non-printing but were still identifiable in the actinic images. The actinic data, complimentary to optical inspection, provides guidance for the potential need for an actinic patterned mask inspection tool to ensure that mask blank printable defects are captured prior to wafer print validation.

SHARP imaging was also performed on a second mask GREMLIN4-LT to provide additional data for validation of the results of the GREMLIN3-PR mask. The GREMLIN4-LT mask blank had a total of 66 Ru defects, identified by the M1350. We intentionally selected a blank with a relatively high level of defectivity to enable better understanding and to classify any new types of defects that have not been observed previously. The automated optical mask and wafer

inspection results showed that only 8 blank defects printed which were of large sizes (> 150 nm). These results have been recently reported [10]. However, one phase defect was identified using wafer printability only—it was not captured by pattern mask inspection. Actinic imaging identified 28 mask blank defects in the patterned areas. This is significantly higher than 8 defects mapped using the automated optical inspection. Unlike wafer prints, SHARP images are continuous grayscale in intensity, and the observed defects had a strong, predictive correlation with the printed results: where the defect contrast was higher, wafer defects were bridged; and where the contrast was lower, defects caused either partial bridging or extensions. Figure 2 contains wafer-print and SHARP images of the same two defects, side-by-side. We believe that partial-bridging or lower contrast defects seen on SHARP are more appropriate for defect compensations using absorber trimming. Likewise, higher contrast defects may be more appropriate for the pattern shift strategy where defects are concealed under absorber regions.

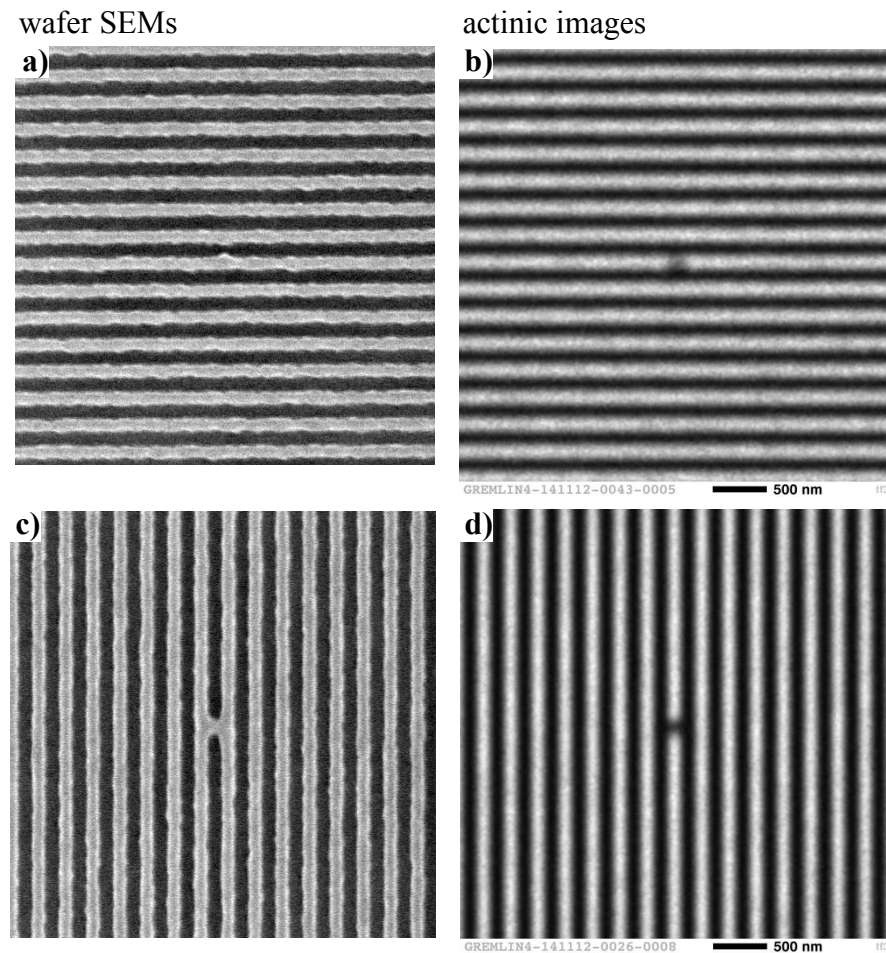wafer SEMs   actinic images

Figure 2. Unbridged (a, b) and bridged (c, d) defects, comparing wafer prints (a, c) to actinic images (b, d) respectively.

Figure 3 shows one defect that was clearly identified as phase defect. It was identified in the wafer print but missed on the mask in optical inspection. Twenty-four blank defects were not

found with SHARP, of which, the majority were in the 1–8 pixel range (100-nm in size). This may be due to the facts that (1) many of these were in the absorber area, and (2) they could be false defects identified in blank inspection. However, SHARP was able to revalidate the inspection of blank defects in the un-patterned area. Four defects were identified by SHARP but not printed or detected on the wafer. Figure 4 shows the distributions of mask blank defects correlated to wafer print and mask blank defect maps.
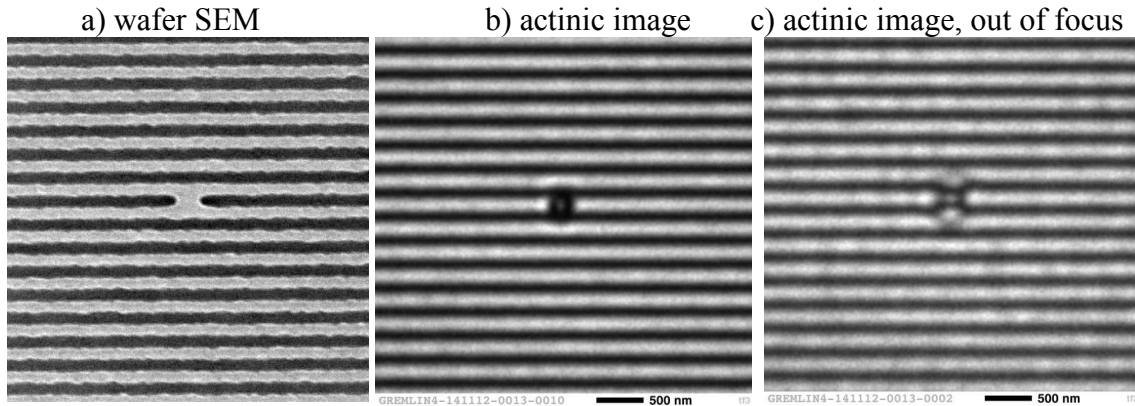

Figure 3. Comparison of wafer SEM and actinic images. The through-focus behavior of the defect in the actinic images shows that this defect has phase-shifting properties in addition to amplitude changes.
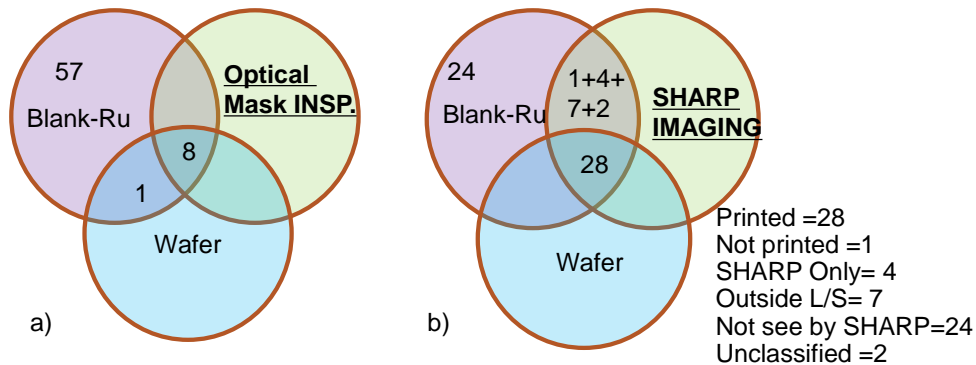

Figure 4. Comparison of mask images, correlated using optical vs. actinic imaging.

Additionally, actinic review reveals the impact of multilayer damage and depicts the printability profile, which can be used as an added metric to define the patterned mask repair and defect compensation strategies. Figure 5 shows an actinic image, mask SEM image and the wafer print of one defect. Without the actinic imaging, it will be difficult to link the mask SEM image of defect to the wafer print, as the magnitude of the printed defect is significantly different. But, once the actinic image is compared, the defect can be correlated. Furthermore, damage to the multilayer reflectivity is captured both by the SHARP and wafer print but is not evident in the mask SEM imaging. Such additional information is clearly helpful to define mitigation strategies.

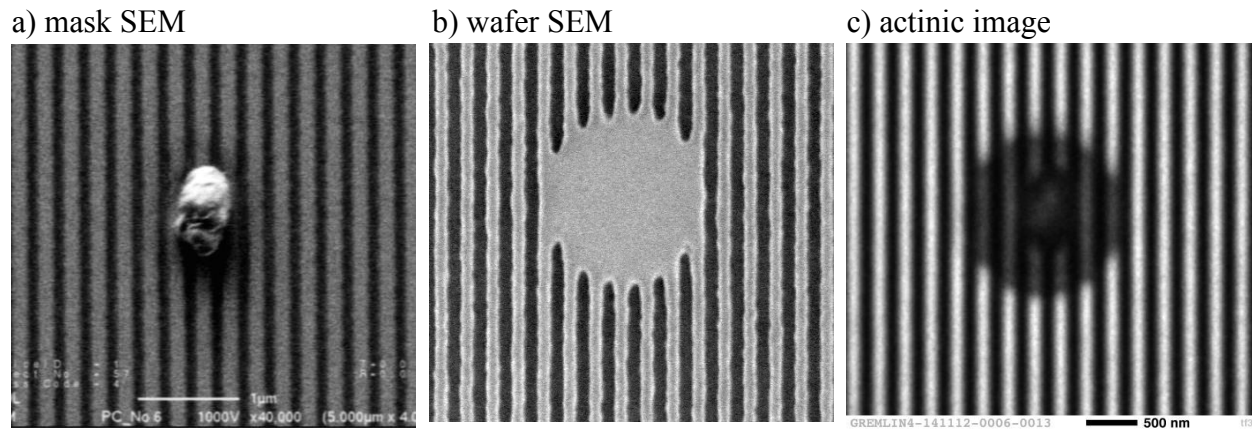a) mask SEM b) wafer SEM c) actinic image

Figure 5. Comparison of (a) mask SEM, (b) wafer SEM, and (c) actinic imaging of a large defect, revealing that the actinic image captures fine details not seen by mask SEM.

4. SUMMARY

Using two masks, defects found by inspection of the Ru-capped EUV blank were correlated with images from the SHARP actinic microscope and SEM imaging of the printed wafers. Actinic imaging predicted wafer printability, down to the fine details of defect shape and intensity changes, and captured a majority of the mask blanks' native defects in the patterned area, compared to automated optical wafer and mask inspections. Furthermore, numerous small defects rated as pixel values 1–4 (< 60 nm) by M1350 blank inspection, were captured and found to be printable. These small defects must be included in defect mitigation strategies either through pattern shift or defect compensation. We observed that the actinic image intensity profiles from the SHARP microscope can be linked to the bridged or unbridged (extensions) lines in the wafer prints, thus providing guidance to either compensate or hide the defects during the mask-making process. Furthermore, blank defects can be detected in both the reflective and the dark, absorber regions of the patterned mask, using SHARP. These results demonstrate that actinic bright field imaging is effective for defect review and for judging defect size, shape, and severity for potential repair. Having a bright field actinic imaging tool will enable defect-free printability in high volume manufacturing with confidence. The SHARP tool is a research prototype that provides a necessary foundation for future development of actinic inspection and imaging of patterned masks.

5. ACKNOWLEDGEMENTS

6. REFERENCES

[1].U. Okoroanyanwu, O. Wood, B. LaFontaine, P. Ackman, A. Tchikoulaeva, K. Bubke, C.Holfeld, J.-H. Peters, S. Kini, S. Watson, I. Lee, M. Bu, P. Lim, S. Raghunathan, C. Boye, "Assessing EUV mask defectivity," *Proc. SPIE* **7636,** 76360J (2010).

[2] A. Tchikoulaeva, U. Okoroanyanwu, O. Wood, B. La Fontaine, C. Holfeld, S. Kini, M. Pelkert, C. Boye, C.-S. Koay, K. Petrillo, H. Mizuno, "EUV reticle defectivity evaluation," *Proc. SPIE* **7271**, 727117 (2009).

[3] C. Higgins, E. Verduijn, X. Hu, L. Wang, M. Singh, J. Wandell, S. Mehta, *et al.* "Integration of an EUV metal layer: a 20/14nm demo," *Proc. SPIE* **9048**, 90481Q (2014).

[4] K. Badger, E. Gallagher, K. Seki, G. McIntyre, T. Konishi, Y. Kodera, and V. Redding. "Evaluation of non-actinic EUV mask inspection and defect printability on multiple EUV mask absorbers," *Proc. SPIE* **8701**, 870114 (2013).

[5] A. Tchikoulaeva, M. Hiroki, S. Tomohiro, T. Kiwamu, K. Haruhiko, Y. Takeshi, T. Tsuneo, W. Hidehiro, I. Soichi, and M. Ichiro. "EUV actinic blank inspection: from prototype to production," *Proc. SPIE* **8697**, 86790I, (2013).

[6] M. Weiss, D. Hellweg, J H Peters, S. Perlitz, A. Garetto, and M. Goldstein. "Actinic review of EUV masks: first results from the AIMS EUV system integration." *Proc. SPIE* **9048**, 90480X, (2014).

[7] A. Barty, K. A. Goldberg, P. Kearney, S. B. Rekawa, B. LaFontaine, O. Wood II, J. S. Taylor and H.-S. Han, "Multilayer defects nucleated by substrate pits: a comparison of actinic inspection and non-actinic inspection techniques," *Proc. SPIE* **6349**, 63492M (2006).

[8] K. A. Goldberg, I. Mochi, M. Benk, A. P. Allezy, M. R. Dickinson, C. W. Cork, D. Zehm, J. B. Macdougall, E. Anderson, F. Salmassi, W. L. Chao, V. K. Vytla, E. M. Gullikson, J. C. DePonte, M. S. Jones, D. Van Camp, J. F. Gamsby, W. B. Ghiorso, H. Huang, W. Cork, E. Martin, E. Van Every, E. Acome, V. Milanovic, R. Delano, P. P. Naulleau, and S. B. Rekawa, "Commissioning an EUV mask microscope for lithography generations reaching 8 nm," *Proc. SPIE* **8679**, 867919 (2013).

[9] U. Okoroanyanwu, J. Heumann, X. Zhu, C. H. Clifford, F. Jiang, P. Mangat, R. Ghaskadavi, *et al*. "Towards the optical inspection sensitivity optimization of EUV masks and EUVL-exposed wafers." *Proc. SPIE* **8352**, 83520V (2012).

[10] E. Verduijn, Private communication, IMEC PTW, Oct 2014.

[11] I. Mochi, K. A. Goldberg, R. Xie, P.-Y. Yan, K. Yamazoe, "Quantitative evaluation of mask phase defects from through-focus EUV aerial images," *Proc. SPIE* **7969**, 79691X (2011).

[12] M. Lawliss, E. Gallagher, M. Hibbs , K. Seki, T. Isogawa, T. Robinson, J. LeClaire, "Repairing native defects on EUV mask blanks," *Proc. SPIE* **9235**, 923516 (2014).